A Model-Based Strategy With Robust Parameter Mismatch for Online HRC Diagnosis and Location in PMSM Drive System

Jun Hang, *Member, IEEE*, Jibo Zhang, Shichuan Ding, *Member, IEEE*, Yourui Huang, and Qunjing Wang, *Member, IEEE*

***Abstract*—This article proposes a model-based strategy with robust parameter mismatch for online high resistance connection (HRC) diagnosis and localization in surface-mounted permanent magnet synchronous machine (PMSM) drive system. The mathematical mode of the PMSM with the HRC is established in the *abc* stationary frame and *dq* rotating frame. Based on the model, the voltage distortion estimator is applied to estimate the voltage distortions caused by the HRC. According to the voltage distortions, a new fault characteristic signal is defined and is analyzed under different fault conditions. Based on the defined signal, the fault indicators being insensitive to the parameter mismatch are defined to diagnose the fault and locate the faulty phases. By the proposed method, not only the HRC can be detected, but also the fault severity can be assessed and the faulty phases can be located, where no additional equipment or measurement devices are needed. Both the simulation and experimental results verify that the proposed method can effectively achieve online HRC diagnosis and location in the PMSM drive system.**

***Index Terms*—Estimator, fault diagnosis, high-resistance connection, permanent magnet synchronous machine (PMSM).**

I. Introduction

VARIABLE-SPEED drive has been widely used in the industrial applications. In particular, permanent magnet synchronous machine (PMSM) drive systems are attracting more and more attention due to their advantages of high efficiency, high torque density, and low volume [1]–[3]. However, a variety of the fault may occur in the PMSM drive system, mainly including the electrical fault, mechanical fault, and demagnetization fault [4]. Among them, high-resistance connection (HRC) is a common electrical fault for the industrial electrical machine [5], [6]. Failure at the joints due to excessive localized heating in HRC, as shown in Fig. 1, is one of the leading root causes of failures in industrial electrical distribution systems [5]. HRC can be caused by a combination of poor workmanship, thermal cycling and vibration, or damage of the contact surfaces due to pitting, corrosion, or contamination. The HRC may lead to the increased torque pulsation, increased losses and excessive heating. As the electric fault is not diagnosed in time, its propagation can cause serious unexpected consequence. Hence, the fault diagnosis is necessarily required to preventing serious damages from happening and improving the reliability of the electrical machine [4].

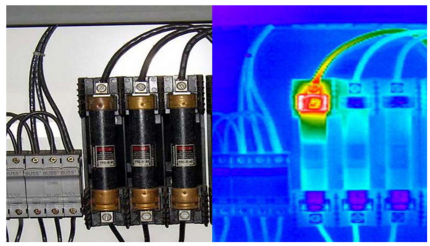

Fig. 1. Overheating at a fuse joint in the electrical distribution system due to HRC [5].

So far, many fault diagnosis methods are proposed for the PMSM, mainly focusing on short-circuit fault [7]–[10], static/dynamic eccentricity [13]–[15], partial/uniform demagnetization [16]–[19], and open-phase fault [20]–[22], while the research on the HRC is relatively few for the PMSM drive system. The studies on the HRC first started with induction machine [4]. In recent years, the HRC fault diagnosis in the PMSM drive system attracts the related researchers' attentions. In [23] and [24], the stator currents and zero-sequence voltage component (ZSVC) are proposed for the HRC diagnosis. In [25], an improved fault indicator and angle difference are analyzed to accomplish the HRC fault detection and location. In [26], the stator current and zero-sequence current component are applied to diagnose the HRC. In [27], the power signature and stator currents are studied to diagnose the HRC. By the methods proposed in [23]–[27], the fault severity cannot be

Manuscript received January 8, 2020; accepted February 20, 2020. Date of publication March 3, 2020; date of current version June 23, 2020. This work was supported in part by the National Natural Science Foundation of China under Grants 51637001 and 51607001, in part by the Natural Science Foundation of Anhui Province under Grant 1708085QE108, and in part by the Science and Technology Project of Guangxi Power Grid (0401002018030103WX00100). Recommended for publication by Associate Editor J. Hur. *(Corresponding author: Jun Hang.)*

Jun Hang, Jibo Zhang, Shichuan Ding, and Qunjing Wang are with the School of Electrical Engineering and Automation, and also with the National Engineering Laboratory of Energy-saving Motor & Control Technique, Anhui University, Hefei 230601, China (e-mail: jun_hang511@163.com; 2541682389@qq.com; dingsc@126.com; wangqunjing@ahu.du.cn).

Yourui Huang is with the School of Electrical and Information Engineering, Anhui University of Science and Technology, Huainan 232001, China (e-mail: hyr628@163.com).

Color versions of one or more of the figures in this article are available online at http://ieeexplore.ieee.org.

Digital Object Identifier 10.1109/TPEL.2020.2978139

quantitatively estimated, especially for the HRC occurring in more than one phase. In [28], the fault severity can be quantitatively estimated, however, the faulty phases are required to be known in advance. In [29], the fault severity is estimated by the resistance deviations calculated from the equation group established using the relationship between the stator currents, ZSVC, and resistance deviations. In [30], a dc-flux-injection method is proposed for HRC fault diagnosis in direct-torque-controlled PMSM drive system. In [31], a new technique is proposed for detecting and classifying turn fault and HRC fault by utilizing both the high- and low-frequency components of the ZSVC, where the dependence on the operating conditions is minimized with the proposed fault indicators. In [32], a new detection and classification algorithm is described for the turn fault and HRC fault based on high-frequency impedance and high-frequency pulsewidth modulation (PWM) ripple current. The methods proposed in [29]–[32] can effectively achieve the HRC diagnosis, fault severity estimation, or location of the faulty phases. However, the extra voltage sensor and balanced resistor network are required, thus leading to the increase of the cost of fault diagnosis and reducing the reliability of fault diagnosis.

The aim of this article is to propose a model-based strategy with robust parameter mismatch for online HRC diagnosis and localization for the surface-mounted PMSM drive system, where the voltage distortion estimator is applied to estimate the voltage distortions. The proposed method not only can detect the HRC, but also can estimate the fault severity and identify the faulty phases, and the proposed method does not need additional equipment or measurement devices, thus reducing the cost of fault diagnosis and reducing the reliability of fault diagnosis. The remainder of this article is organized as follows. In Section II, the mathematical model of the PMSM with HRC is established under different conditions. In Section III, the detailed fault diagnosis process is described. In Section IV, the influence of the parameter mismatch on the fault diagnosis performance is analyzed. In Sections V and VI, both the simulation and experiment platform are established to validate the proposed method, respectively. Finally, the conclusion is drawn in Section VII.

II. PMSM Model

A. PMSM Model Under Healthy Condition

Neglecting the saturation, the voltage equations of the healthy PMSM are expressed as follows:

$$\begin{cases} u_d = R_s i_d + L_d \dfrac{d}{dt} i_d - \omega_e L_q i_q \\ u_q = R_s i_q + L_q \dfrac{d}{dt} i_q + \omega_e L_d i_d + \omega_e \psi_f \end{cases} \tag{1}$$

where u_d and u_q the are *dq*-axis voltages under healthy condition, i_d and i_q are the *dq*-axis stator currents, L_d and L_q are the *dq*-axis inductances, R_s is the stator resistance, ψ_f is permanent magnet (PM) flux linkage, and ω_e is the electrical angle frequency.

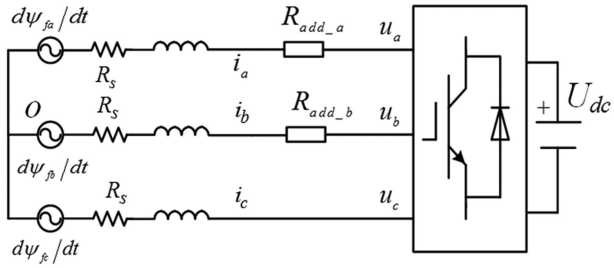

Fig. 2. Equivalent model of PMSM with HRC fault.

B. PMSM Model Under Fault Condition

1) Stationary Frame: As the HRC occurs in the PMSM drive system, as shown in Fig. 2, the voltage equation for three-phase PMSM in the *abc* stationary frame can be expressed as follows:

$$[u_{abc}] = [R_{sf}][i_{abc}] + [L_{sf}]\frac{d}{dt}[i_{abc}] + [e_{abc}] \tag{2}$$

where $[u_{abc}] = [u_a,\, u_b,\, u_c]^T$ is the stator voltage matrix, $[i_{abc}] = [i_a,\, i_b,\, i_c]^T$ is the stator current matrix, $[L_s]$ is the stator winding inductance matrix, $[R_{sf}]$ is the stator winding resistance matrix, and $[e_{abc}] = [e_a,\, e_b,\, e_c]^T$ is the no-load electromotive force matrix. In addition, $[L_s]$ and $[e_{abc}]$ are respectively expressed as follows:

$$[L_s] = \begin{bmatrix} L & M & M \\ M & L & M \\ M & M & L \end{bmatrix}$$

$$[e_{abc}] = \frac{d}{dt}\begin{bmatrix} \psi_{fa} \\ \psi_{fb} \\ \psi_{fc} \end{bmatrix} = \frac{d}{dt}\begin{bmatrix} \psi_f \cos(\theta) \\ \psi_f \cos\left(\theta - \dfrac{2\pi}{3}\right) \\ \psi_f \cos\left(\theta + \dfrac{2\pi}{3}\right) \end{bmatrix}.$$

As the HRC fault occurs in phase b, $[R_{sf}]$ is expressed as follows:

$$[R_{sf}] = \begin{bmatrix} R_s & 0 & 0 \\ 0 & R_s + R_{\mathrm{add\_}b} & 0 \\ 0 & 0 & R_s \end{bmatrix}.$$

Similarly, as the HRC fault occurs in the phases a and b simultaneously, $[R_{sf}]$ is expressed as follows:

$$[R_{sf}] = \begin{bmatrix} R_s + R_{\mathrm{add\_}a} & 0 & 0 \\ 0 & R_s + R_{\mathrm{add\_}b} & 0 \\ 0 & 0 & R_s \end{bmatrix}$$

where R_s is the phase resistance, L is the stator phase self-inductance, M is the mutual-inductance between the stator phases, θ is the rotor electrical position, and $R_{\mathrm{add\_}a}$ and $R_{\mathrm{add\_}b}$ are the additional resistances in the stator windings of the phase a and phase b, respectively.

2) Rotating Frame: As the HRC occurs in phase *b*, applying Park's transform to (2) yields

$$\begin{cases} u_{d\_f} = \left(R_s + \frac{2}{3}R_{\text{add\_}b}\cos^2\left(\theta - \frac{2\pi}{3}\right)\right) i_d \\ \qquad -\frac{2}{3}R_{\text{add\_}b}\sin\left(\theta - \frac{2\pi}{3}\right)\cos\left(\theta - \frac{2\pi}{3}\right) i_q \\ \qquad + L_d\frac{di_d}{dt} - \omega_e L_q i_q \\ u_{q\_f} = -\frac{2}{3}R_{\text{add\_}b}\sin\left(\theta - \frac{2\pi}{3}\right)\cos\left(\theta - \frac{2\pi}{3}\right) i_d \\ \qquad + \left(R_s + \frac{2}{3}R_{\text{add\_}b}\sin^2\left(\theta - \frac{2\pi}{3}\right)\right) i_q + L_q\frac{di_q}{dt} \\ \qquad + \omega_e L_d i_d + \omega_e \psi_f \end{cases} \tag{3}$$

where u_{d_f} and u_{q_f} are *dq*-axis voltages under fault condition. L_d and L_q are the *dq*-axis inductance, and $L_d = L_q = L–M$.

Similarly, as the HRC fault occurs in phases *a* and *b*, applying Park's transform to (2) yields

$$\begin{cases} u_{d\_f} = \left(R_s + \frac{2}{3}R_{\text{add\_}a}\cos^2\theta + \frac{2}{3}R_{\text{add\_}b}\cos^2\left(\theta - \frac{2\pi}{3}\right)\right) i_d \\ \qquad - \left(\frac{2}{3}R_{\text{add\_}a}\sin\theta\cos\theta + \frac{2}{3}R_{\text{add\_}b}\sin\left(\theta - \frac{2\pi}{3}\right)\right. \\ \qquad \left.\cos\left(\theta - \frac{2\pi}{3}\right)\right) i_q + L_d\frac{di_d}{dt} - \omega_e L_q i_q \\ u_{q\_f} = -\left(\frac{2}{3}R_{\text{add\_}a}\sin\theta\cos\theta\right. \\ \qquad \left. + \frac{2}{3}R_{\text{add\_}b}\sin\left(\theta - \frac{2\pi}{3}\right)\cos\left(\theta - \frac{2\pi}{3}\right)\right) i_d \\ \qquad + \left(R_s + \frac{2}{3}R_{\text{add\_}a}\sin^2\theta + \frac{2}{3}R_{\text{add\_}b}\sin^2\left(\theta - \frac{2\pi}{3}\right)\right) i_q \\ \qquad + L_q\frac{di_q}{dt} + \omega_e L_d i_d + \omega_e \psi_f. \end{cases} \tag{4}$$

Based on (1), (3) can be rewritten as follows:

$$\begin{cases} u_{d\_f} = u_d + \Delta u_d \\ u_{q\_f} = u_q + \Delta u_q \end{cases} \tag{5}$$

where Δu_d and Δu_q are the *dq*-axis voltage deviations due to the HRC, and Δu_d and Δu_q are expressed as follows:

$$\begin{cases} \Delta u_d = \frac{2}{3}R_{\text{add\_}b} i_d \cos^2\left(\theta - \frac{2\pi}{3}\right) \\ \qquad -\frac{2}{3}R_{\text{add\_}b} i_q \sin\left(\theta - \frac{2\pi}{3}\right)\cos\left(\theta - \frac{2\pi}{3}\right) \\ \Delta u_q = -\frac{2}{3}R_{\text{add\_}b} i_d \sin\left(\theta - \frac{2\pi}{3}\right)\cos\left(\theta - \frac{2\pi}{3}\right) \\ \qquad +\frac{2}{3}R_{\text{add\_}b} i_q \sin^2\left(\theta - \frac{2\pi}{3}\right). \end{cases} \tag{6}$$

Similarly, as the HRC fault occurs in phases *a* and *b*, Δu_d and Δu_q are expressed as follows:

$$\begin{cases} \Delta u_d = \left(\frac{2}{3}R_{\text{add\_}a}\cos^2\theta + \frac{2}{3}R_{\text{add\_}b}\cos^2\left(\theta - \frac{2\pi}{3}\right)\right) i_d \\ \qquad - \left(\frac{2}{3}R_{\text{add\_}a}\sin\theta\cos\theta + \frac{2}{3}R_{\text{add\_}b}\sin\left(\theta - \frac{2\pi}{3}\right)\right. \\ \qquad \left.\cos\left(\theta - \frac{2\pi}{3}\right)\right) i_q \\ \Delta u_q = -\left(\frac{2}{3}R_{\text{add\_}a}\sin\theta\cos\theta + \frac{2}{3}R_{\text{add\_}b}\sin\left(\theta - \frac{2\pi}{3}\right)\right. \\ \qquad \left.\cos\left(\theta - \frac{2\pi}{3}\right)\right) i_d \\ \qquad + \left(\frac{2}{3}R_{\text{add\_}a}\sin^2\theta + \frac{2}{3}R_{\text{add\_}b}\sin^2\left(\theta - \frac{2\pi}{3}\right)\right) i_q. \end{cases} \tag{7}$$

It can be seen from (4)–(7) that the stator voltages after fault occurrence can be represented as two parts. One is the normal *dq*-axis voltages and the other is the *dq*-axis voltage deviations caused by the HRC. In addition, the analysis for the HRC in other phase can be made in a similar manner.

III. Fault Diagnosis and Location

To achieve the HRC diagnosis and location, a simple and low-cost fault diagnosis algorithm is proposed based on the voltage distortion estimator and it does not require any additional hardware circuits. The voltage distortions due to the HRC in the *dq*-axis reference frame are estimated based on the electrical model of the PMSM. Based on the voltage distortions, the new fault characteristic signal is defined to achieve the HRC diagnosis and location.

A. Voltage Distortion Estimation

The current dynamics of a PMSM including the voltage distortions caused by HRC can be represented as follows:

$$\begin{bmatrix} \frac{di_d}{dt} \\ \frac{di_q}{dt} \end{bmatrix} = \begin{bmatrix} -\frac{R_s}{L_d} & \frac{\omega_e L_q}{L_d} \\ -\frac{\omega_e L_d}{L_q} & -\frac{R}{L_d} \end{bmatrix} \begin{bmatrix} i_d \\ i_q \end{bmatrix} + \begin{bmatrix} \frac{1}{L_d} & 0 \\ 0 & \frac{1}{L_q} \end{bmatrix} \begin{bmatrix} u_d + \Delta u_d \\ u_q + \Delta u_q \end{bmatrix} - \begin{bmatrix} 0 \\ \frac{\omega_e \psi_f}{L_q} \end{bmatrix}. \tag{8}$$

As can be seen from (8), the stator currents are affected by the voltage distortions caused by the HRC.

For the reference model, it is assumed that the system is healthy and the voltage distortions are zero. Under this condition, the calculated current dynamics with the rated parameters can be represented as follows [33]:

$$\begin{bmatrix} \frac{di_{dm}}{dt} \\ \frac{di_{qm}}{dt} \end{bmatrix} = \begin{bmatrix} -\frac{R_s}{L_d} & \frac{\omega_e L_q}{L_d} \\ -\frac{\omega_e L_d}{L_q} & -\frac{R}{L_d} \end{bmatrix} \begin{bmatrix} i_d \\ i_q \end{bmatrix} + \begin{bmatrix} \frac{1}{L_d} & 0 \\ 0 & \frac{1}{L_q} \end{bmatrix} \begin{bmatrix} u_d^* - u_d^{\text{dead}} \\ u_q^* - u_q^{\text{dead}} \end{bmatrix} - \begin{bmatrix} 0 \\ \frac{\omega_e \psi_f}{L_q} \end{bmatrix} \tag{9}$$

where u_d^* and u_q^* are the *dq*-axis stator voltage commands, i_{dm} and i_{qm} are the *dq*-axis currents of the PMSM model, u_d^{dead} and u_q^{dead} are the *dq*-axis voltage compensation due to the dead-time effect, and are expressed as follows:

$$\begin{bmatrix} u_d^{\text{dead}} \\ u_q^{\text{dead}} \end{bmatrix} = \frac{2}{3}\begin{bmatrix} \cos\theta & \cos\left(\theta - \frac{2\pi}{3}\right) & \cos\left(\theta + \frac{2\pi}{3}\right) \\ \sin\theta & \sin\left(\theta - \frac{2\pi}{3}\right) & \sin\left(\theta - \frac{2\pi}{3}\right) \end{bmatrix} \begin{bmatrix} u_a^{\text{dead}} \\ u_b^{\text{dead}} \\ u_c^{\text{dead}} \end{bmatrix} \tag{10}$$

where u_a^{dead}, u_b^{dead}, and u_c^{dead} are the voltage compensations in the *abc* stationary frame and are expressed as follows [34]:

$$\begin{cases} u_a^{\mathrm{dad}} = (2\mathrm{sgn}(i_a) - \mathrm{sgn}(i_b) - \mathrm{sgn}(i_c))\, A_p \\ u_b^{\mathrm{dad}} = (2\mathrm{sgn}(i_b) - \mathrm{sgn}(i_c) - \mathrm{sgn}(i_a))\, A_p \\ u_c^{\mathrm{dad}} = (2\mathrm{sgn}(i_c) - \mathrm{sgn}(i_a) - \mathrm{sgn}(i_b))\, A_p \\ A_p = \frac{1}{6}\left(2\left(U_{dc} - U_{ce} + U_d\right)\frac{(t_{\mathrm{dead}} + t_{\mathrm{on}} - t_{\mathrm{off}})}{T_s} + (U_{ce} + U_d)\right) \end{cases} \tag{11}$$

where sgn(·) is a sign function of each phase current, U_{dc} is the dc-link voltage, U_{ce} is the saturation voltage of the active switch, U_d is the forward voltage of the antiparallel diode, T_s is the sample period, t_{dead} is the intended blanking time to prevent the short-circuit phenomenon, t_{on} is the sum of the turn-ON delay and transition time, and t_{off} is the sum of the turn-OFF delay and transition time.

Based on (8) and (9), the voltage distortions due to HRC can be obtained as follows:

$$\begin{cases} \Delta u_d = L_s\left(\frac{di_d}{dt} - \frac{di_{dm}}{dt}\right) - u_d^{\mathrm{dead}} \\ \Delta u_q = L_s\left(\frac{di_q}{dt} - \frac{di_{qm}}{dt}\right) - u_q^{\mathrm{dead}} \end{cases} \tag{12}$$

where $L_s = L_d = L_q$.

Then the average voltage distortions over k_{th} PWM step can be derived from (12) and can be expressed as follows:

$$\begin{cases} \Delta u_d = L_s\left(\frac{i_d(k) - i_{dm}(k)}{T_s}\right) - u_d^{\mathrm{dead}} \\ \Delta u_q = L_s\left(\frac{i_q(k) - i_{qm}(k)}{T_s}\right) - u_q^{\mathrm{dead}}. \end{cases} \tag{13}$$

The model current $i_{dm}(k)$ and $i_{qm}(k)$ in (13) can be obtained from the discrete form of (9) and are expressed as follows:

$$\begin{aligned} \begin{bmatrix} i_{dm}(k) \\ i_{qm}(k) \end{bmatrix} = & \begin{bmatrix} 1 - \frac{R_s}{L_d}T & T_s\frac{\omega_e(k-1)L_q}{L_d} \\ -T_s\frac{\omega_e(k-1)L_d}{L_q} & 1 - \frac{R}{L_d} \end{bmatrix} \begin{bmatrix} i_d(k-1) \\ i_q(k-1) \end{bmatrix} \\ & + \begin{bmatrix} \frac{1}{L_d} & 0 \\ 0 & \frac{1}{L_q} \end{bmatrix} \begin{bmatrix} u_d^*(k-1) - u_d^{\mathrm{dead}}(k-1) \\ u_q^*(k-1) - u_q^{\mathrm{dead}}(k-1) \end{bmatrix} \\ & - \begin{bmatrix} 0 \\ T_s\frac{\omega_e(k-1)\psi_f}{L_q} \end{bmatrix} \end{aligned} \tag{14}$$

where k and $(k-1)$ means the kth and $(k-1)$th sample, respectively.

B. Fault Characteristic Signal

It can be seen from (6) and (7) that the HRC can lead to the *dq*-axis voltage deviations. Theoretically, the HRC can be diagnosed by the *dq*-axis voltage deviations. However, as is known from (6) and (7), the *dq*-axis voltage deviations contanins more fault information, such as the additional resistance R_{add}, stator currents (i_d, i_q) and trigonometric function. As only the voltage deviation Δu_d or Δu_q is used, the HRC can be monitored. However, the faulty phases cannot be located and the fault severity cannot be easily estimated, especially for the HRC in two phases. Moreover, it can be seen that there is a certain degree of symmetry for the *dq*-axis voltage deviation Δu_d or Δu_q. Therefore, it is hoped that both the *dq*-axis voltage deviations Δu_d and Δu_q are used, and a simpler and more effective signal can be constructed based on Δu_d and Δu_q. Based on this idea, to effectively achieve the fault detection and location, the new fault characteristic signal F_{sum} is defined as follows:

$$F_{\mathrm{sum}} = \Delta u_d i_q + \Delta u_q i_d. \tag{15}$$

For the HRC in phase *b*, by substituting (6) into (15), it has

$$\begin{aligned} F_{\mathrm{sum}} = & \left(\frac{2}{3}R_{\mathrm{add\_}b} i_d \cos^2\left(\theta - \frac{2\pi}{3}\right)\right. \\ & \left. - \frac{2}{3}R_{\mathrm{add\_}b} i_q \sin\left(\theta - \frac{2\pi}{3}\right)\cos\left(\theta - \frac{2\pi}{3}\right)\right) i_q \\ & + \left(-\frac{2}{3}R_{\mathrm{add\_}b} i_d \sin\left(\theta - \frac{2\pi}{3}\right)\cos\left(\theta - \frac{2\pi}{3}\right)\right. \\ & \left. + \frac{2}{3}R_{\mathrm{add\_}b} i_q \sin^2\left(\theta - \frac{2\pi}{3}\right)\right) i_d \\ = & \frac{2}{3}R_{\mathrm{add\_}b} i_d i_q \left(\cos^2\left(\theta - \frac{2\pi}{3}\right) + \sin^2\left(\theta - \frac{2\pi}{3}\right)\right) \\ & - \frac{2}{3}R_{\mathrm{add\_}b}\left(i_d^2 + i_q^2\right)\sin\left(\theta - \frac{2\pi}{3}\right)\cos\left(\theta - \frac{2\pi}{3}\right) \\ = & \frac{2}{3}R_{\mathrm{add\_}b} i_d i_q + \frac{1}{3}R_{\mathrm{add\_}b}\left(i_d^2 + i_q^2\right)\sin\left(2\theta - \frac{\pi}{3}\right) \\ = & F_{\mathrm{dc}} + F_2 \sin\left(2\theta + \theta_f\right) \end{aligned} \tag{16}$$

where F_{dc} is the dc component in F_{sum}, F_2 and θ_f are the amplitude and the initial phase angle of the second harmonic component in F_{sum}, respectively, and are expressed as follows:

$$\begin{cases} F_{\mathrm{dc}} = \frac{2}{3}R_{\mathrm{add\_}b} i_d i_q \\ F_2 = \frac{1}{3}R_{\mathrm{add\_}b}(i_d^2 + i_q^2) \\ \theta_f = -\frac{\pi}{3}. \end{cases} \tag{17}$$

According to (17), it can be seen that the amplitude F_{dc} and F_2 are linear proportional to the additional resistance $R_{\mathrm{add\_}b}$ as i_d and i_q are unvaried. Hence, dc component and second harmonic component in the fault characteristic signal F_{sum} could be used to detect the HRC.

Similarly, as the HRC fault occurs in the phases *a* and *b*, by substituting (7) into (15), it has

$$\begin{aligned} F_{\mathrm{sum}} = & \frac{2}{3}\left(R_{\mathrm{add\_}a} + R_{\mathrm{add\_}b}\right) i_d i_q + \frac{1}{3}\left(i_d^2 + i_q^2\right) \\ & \times \left(R_{\mathrm{add\_}a}\sin\left(2\theta + \pi\right) + R_{\mathrm{add\_}b}\sin\left(2\theta - \frac{\pi}{3}\right)\right) \\ = & F_{\mathrm{dc}} + F_2\sin\left(2\theta + \theta_f\right) \end{aligned} \tag{18}$$

where $F_{\rm dc}$, F_2 and θ_f are expressed as follows:

$$\begin{cases} F_{\rm dc} = \frac{2}{3}(R_{\rm add\_}a + R_{\rm add\_}b) i_d i_q \\ F_2 = \frac{1}{3}\left(i_d^2 + i_q^2\right)\sqrt{R_{\rm add\_}a^2 + R_{\rm add\_}b^2 - R_{\rm add\_}a R_{\rm add\_}b} \\ \theta_f = \arcsin\left(-\frac{\sqrt{3}}{2}\frac{R_{\rm add\_}b}{\sqrt{R_{\rm add\_}a^2 + R_{\rm add\_}b^2 - R_{\rm add\_}a R_{\rm add\_}b}}\right). \end{cases} \tag{19}$$

It can be seen from (19) that the initial phase angle θ_f is determined by $R_{\rm add\_}a$ and $R_{\rm add\_}b$.

C. Fault Indicator

As discussed in Section III-B, the HRC could be detected by DC component and second harmonic component in $F_{\rm sum}$. However, as the common $i_d = 0$ method is used to control the PMSM, the $F_{\rm dc}$ will be equal to 0 and cannot be used to detect the HRC. Hence, in this paper, the second harmonic component in $F_{\rm sum}$ is applied.

As the fault occurs in the phase b, according to (16), the amplitude of the second harmonic component in the $F_{\rm sum}$ can be expressed as follows:

$$F_2 = \frac{1}{3} R_{\rm add\_}b \left(i_d^2 + i_q^2\right). \tag{20}$$

The additional resistance can be estimated as follows:

$$R_{{\rm add},e} = \frac{3F_2}{i_d^2 + i_q^2} \tag{21}$$

where $R_{{\rm add},e}$ is the estimated resistance. Combining (20) and (21), it can be seen that $R_{{\rm add},e}$ is not affected by the stator current of the PMSM since the quantities sensitive to i_d and i_q in the numerator and denominator of the right-hand side of (20) are eliminated. Furthermore, it is obvious that the value of $R_{{\rm add},e}$ is theoretically equal to the value of $R_{\rm add\_}b$.

As the HRC occurs in phases *a* and *b* simultaneously, according to (19), F_2 can be expressed as follows:

$$\begin{aligned} F_2 &= \frac{1}{3}\left(i_d^2 + i_q^2\right)\sqrt{R_{\rm add\_}a^2 + R_{\rm add\_}b^2 - R_{\rm add\_}a R_{\rm add\_}b} \\ &= \frac{1}{3}\left(i_d^2 + i_q^2\right) R_{{\rm add},e} \end{aligned} \tag{22}$$

where $R_{{\rm add},e}$ is expressed as follows:

$$R_{{\rm add},e} = \sqrt{R_{\rm add\_}a^2 + R_{\rm add\_}b^2 - R_{\rm add\_}a R_{\rm add\_}b}. \tag{23}$$

And $R_{{\rm add},e}$ can be calculated by the following equation:

$$R_{{\rm add},e} = \frac{3F_2}{i_d^2 + i_q^2}. \tag{24}$$

Combining (22) and (24), it can be seen that $R_{{\rm add},e}$ is not affected by the stator currents of the PMSM since the quantities sensitive to i_d and i_q are canceled out.

According to (21) and (24), it can be seen that the expressions of the estimated resistance are the same no matter the HRC occurs in single phase *a* or two phases *a* and *b*. Hence, $R_{{\rm add},e}$ can be regarded as a reliable fault indicator, which is not affected by the stator currents and not limited by the faulty phases.

TABLE I
INITIAL PHASE ANGLE UNDER DIFFERENT FAULT CONDITIONS

Case		θ_f
Fault in the phase *a*		π
Fault in the phase *b*		$-\pi/3$
Fault in the phase *c*		$\pi/3$
Fault in the phases *a* and *b*	$R_{add\_a}=R_{add\_b}$	$-2\pi/3$
	$R_{add\_a}>R_{add\_b}$	$(-\pi \quad -2\pi/3)$
	$R_{add\_a}<R_{add\_b}$	$(-2\pi/3 \quad -\pi/3)$
Fault in the phases *b* and *c*	$R_{add\_b}=R_{add\_c}$	0
	$R_{add\_b}>R_{add\_c}$	$(-\pi/3 \quad 0)$
	$R_{add\_b}<R_{add\_c}$	$(0 \quad \pi/3)$
Fault in the phases *c* and *a*	$R_{add\_c}=R_{add\_a}$	$2\pi/3$
	$R_{add\_c}>R_{add\_a}$	$(\pi/3 \quad 2\pi/3)$
	$R_{add\_c}<R_{add\_a}$	$(2\pi/3 \quad \pi)$

Once the HRC is detected by the fault indicator, and then the faulty phases are required to be identified. In this article, it is proposed that the identification of the faulty phases is implemented by the initial phase angle θ_f. Based on (17) and (19), it can be known that the initial phase angle θ_f is equal to -60 as the fault is just appeared in the phase *b*, and the initial phase angle θ_f is between –180 and –60 as the fault occurs in two phases *a* and *b*. Additionally, the similar results can be obtained in the case of the HRC fault in other phases. Table I lists the theoretical values of the initial phase angle θ_f under different HRC conditions, indicating that the angle θ_f can be used to identify the faulty phases.

D. Frequency Tracking Algorithm

In order to achieve online diagnosis of the HRC, it is necessary to obtain the fault indicator in real time since one may not know the moment that the HRC would aggravate to the extent leading to machine breakdown. As seen from (17), (19), (21), and (24), only F_2 and θ_f are required to be extracted in real time to calculate the fault indicator since the *dq*-axis currents i_d and i_q can be directly obtained from the PMSM control system. Hence, the frequency tracking algorithm is applied to calculate the amplitude and initial phase angle [25]. The detailed processes are given as follows.

No matter the HRC occurs in one phase or two phases, according to (16) and (18), it is known that the fault characteristic signal $F_{\rm sum}$ can be expressed as follows:

$$F_{\rm sum} = F_{\rm dc} + F_2 \sin\left(2\theta + \theta_f\right). \tag{25}$$

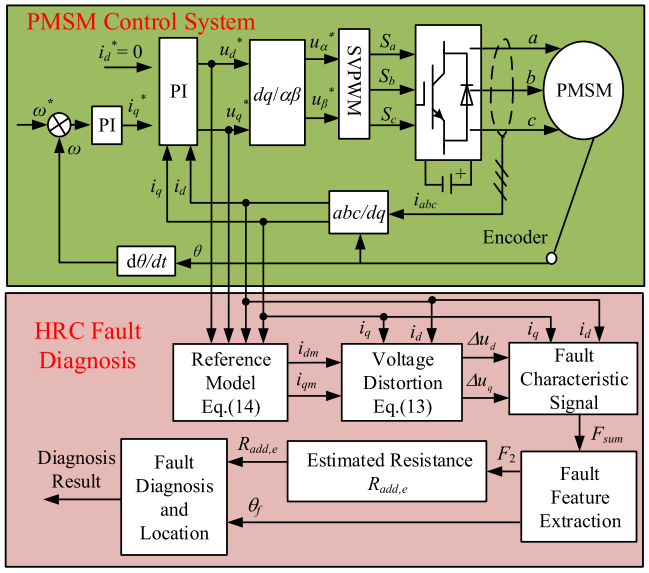

Fig. 3. Configuration of the proposed fault diagnosis method.

First, (25) is transformed into a stationary orthogonal reference frame, and the voltage components are defined as follows:

$$\begin{cases} F_{\text{sum\_}d} = \left(F_{\text{dc}} + F_2 \sin\left(2\theta + \theta_f\right)\right)\cos(2\theta) \\ F_{\text{sum\_}q} = \left(F_{\text{dc}} + F_2 \sin\left(2\theta + \theta_f\right)\right)\sin(2\theta). \end{cases} \tag{26}$$

By using trigonometric identities, (26) can be expressed as follows:

$$\begin{cases} F_{\text{sum\_}d} = F_{\text{dc}}\cos(2\theta) + \frac{1}{2}F_2\left[\sin\left(4\theta + \theta_f\right) + \sin\left(\theta_f\right)\right] \\ F_{\text{sum\_}q} = F_{\text{dc}}\sin(2\theta) + \frac{1}{2}F_2\left[\cos\left(4\theta + \theta_F\right) - \cos\left(\theta_f\right)\right]. \end{cases} \tag{27}$$

Then the harmonic components of the voltage signals in (27) is filtered out by a first-order low-pass filter, where the cut-off frequency is set to ω_e based on the expression of (27), and it has

$$\begin{cases} F_{\text{sum\_}dl} = \frac{1}{2}F_2\sin\left(\theta_f\right) \\ F_{\text{sum\_}ql} = \frac{1}{2}F_2\cos\left(\theta_f\right) \end{cases} \tag{28}$$

where $F_{\text{sum\_}dl}$ and $F_{\text{sum\_}ql}$ are the dc voltage components in $F_{\text{sum\_}d}$ and $F_{\text{sum\_}q}$, respectively. It can be seen from (28) that $F_{\text{sum\_}dl}$ and $F_{\text{sum\_}ql}$ have a direct relationship with the amplitude and initial phase angle of the second harmonic component in F_{sum}. Finally, the amplitude and initial phase angle can be calculated as follows:

$$\begin{cases} F_2 = 2\sqrt{F_{\text{sum\_}dl}^2 + F_{\text{sum\_}ql}^2} \\ \theta_f = \tan^{-1}\left(\frac{F_{\text{sum\_}dl}}{F_{\text{sum\_}ql}}\right). \end{cases} \tag{29}$$

It can be seen from (29) that the amplitude and initial phase angle can be effectively extracted.

E. Fault Diagnosis and Location

Fig. 3 shows the block diagram of the proposed fault diagnosis method. First, the voltage distortions Δu_d and Δu_q are observed from the plant and model currents of the PMSM drive system based on (13) and (14); then the fault characteristic signal F_{sum} is calculated according to (15); next, the fault features F_2 and θ_f are extracted from F_{sum} by the frequency tracking algorithm and the fault indicator can be calculated based on (19) or (22). Finally, the status is judged by comparing the fault indicator with the preset threshold which is corresponding to its value for the healthy PMSM, and then the faulty phases are identified by the angle θ_f.

IV. Analysis of Parameter Mismatch on Fault Diagnosis Performance

As seen from (13) and (14), the voltage distortions are dependent on the parameters of the PMSM, mainly including the stator resistance R_s, dq-axis inductances L_d and L_q, and PM flux linkage ψ_f. As is known, the parameters of the PMSM are affected by the temperature, operating conditions and so on. Hence, it is greatly necessary to analyze the influence of the parameter mismatch on the performance of the proposed fault diagnosis method.

It is supposed that the three-phase resistances vary to $R_s + \Delta R_s$, and the dq-axis inductances vary to $L_d + \Delta L_d$ and $L_q + \Delta L_q$, respectively, and the PM flux linkage varies to $\psi_f + \Delta\psi_f$. As the HRC occurs in phase b, (3) is changed into

$$\begin{cases} u_{d\_f} = \left(R_s + \Delta R_s + \frac{2}{3}R_{\text{add\_}b}\cos^2\left(\theta - \frac{2\pi}{3}\right)\right) i_d \\ \qquad -\frac{2}{3}R_{\text{add\_}b} i_q \sin\left(\theta - \frac{2\pi}{3}\right)\cos\left(\theta - \frac{2\pi}{3}\right) \\ \qquad + \left(L_d + \Delta L_d\right)\frac{di_d}{dt} - \omega_e\left(L_q + \Delta L_q\right) i_q \\ u_{q\_f} = -\frac{2}{3}R_{\text{add\_}b} i_d \sin\left(\theta - \frac{2\pi}{3}\right)\cos\left(\theta - \frac{2\pi}{3}\right) \\ \qquad + \left(R_s + \Delta R_s + \frac{2}{3}R_{\text{add\_}b}\sin^2\left(\theta - \frac{2\pi}{3}\right)\right) i_q \\ \qquad + \left(L_q + \Delta L_q\right)\frac{di_q}{dt} + \omega_e\left(L_d + \Delta L_d\right) i_d \\ \qquad + \omega_e\left(\psi_f + \Delta\psi_f\right). \end{cases} \tag{30}$$

In this case, based on (1), (5), and (30), the voltage distortions Δu_d and Δu_q are obtained as follows:

$$\begin{cases} \Delta u_d = \left(\Delta R_s + \frac{2}{3}R_{\text{add\_}b}\cos^2\left(\theta - \frac{2\pi}{3}\right)\right) i_d + \Delta L_d\frac{di_d}{dt} \\ \qquad -\omega_e\Delta L_q i_q - \frac{2}{3}R_{\text{add\_}b}\sin\left(\theta - \frac{2\pi}{3}\right)\cos\left(\theta - \frac{2\pi}{3}\right) i_q \\ \Delta u_q = -\frac{2}{3}R_{\text{add\_}b} i_d \sin\left(\theta - \frac{2\pi}{3}\right)\cos\left(\theta - \frac{2\pi}{3}\right) + \Delta L_q\frac{di_q}{dt} \\ \qquad + \left(\Delta R_s + \frac{2}{3}R_{\text{add\_}b}\sin^2\left(\theta - \frac{2\pi}{3}\right)\right) i_q + \omega_e\Delta L_d i_d \\ \qquad + \omega_e\Delta\psi_f. \end{cases} \tag{31}$$

As the PMSM operates at a fixed load, the dq-axis currents i_d and i_q are usually constants. Hence, the di_d/dt and di_q/dt are

equal to 0, and (31) can be simplified as follows:

$$\begin{cases} \Delta u_d = \left(\Delta R_s + \frac{2}{3}R_{\text{add\_}b}\cos^2\left(\theta - \frac{2\pi}{3}\right)\right) i_d - \omega_e \Delta L_q i_q \\ \qquad\quad -\frac{2}{3}R_{\text{add\_}b}\sin\left(\theta - \frac{2\pi}{3}\right)\cos\left(\theta - \frac{2\pi}{3}\right) i_q \\ \Delta u_q = -\frac{2}{3}R_{\text{add\_}b} i_d \sin\left(\theta - \frac{2\pi}{3}\right)\cos\left(\theta - \frac{2\pi}{3}\right) \\ \qquad\quad + \left(\Delta R_s + \frac{2}{3}R_{\text{add\_}b}\sin^2\left(\theta - \frac{2\pi}{3}\right)\right) i_q + \omega_e \Delta \psi_f \\ \qquad\quad + \omega_e \Delta L_d i_d. \end{cases} \tag{32}$$

By substituting (32) into (15), it has

$$\begin{aligned} F_{\text{sum}} &= \left(\left(\Delta R_s + \frac{2}{3}R_{\text{add\_}b}\cos^2\left(\theta - \frac{2\pi}{3}\right)\right) i_d - \omega_e \Delta L_q i_q \right. \\ &\quad \left. -\frac{2}{3}R_{\text{add\_}b}\sin\left(\theta - \frac{2\pi}{3}\right)\cos\left(\theta - \frac{2\pi}{3}\right) i_q\right) i_q \\ &\quad + \left(-\frac{2}{3}R_{\text{add\_}b} i_d \sin\left(\theta - \frac{2\pi}{3}\right)\cos\left(\theta - \frac{2\pi}{3}\right)\right. \\ &\quad \left. + \left(\Delta R_s + \frac{2}{3}R_{\text{add\_}b}\sin^2\left(\theta - \frac{2\pi}{3}\right)\right) i_q + \omega_e \Delta \psi_f \right. \\ &\quad \left. + \omega_e \Delta L_d i_d\right) i_d \\ &= \frac{2}{3}R_{\text{add\_}b} i_d i_q \left(\cos^2\left(\theta - \frac{2\pi}{3}\right) + \sin^2\left(\theta - \frac{2\pi}{3}\right)\right) \\ &\quad - \frac{2}{3}R_{add\_b}(i_d^2 + i_q^2)\sin\left(\theta - \frac{2\pi}{3}\right)\cos\left(\theta - \frac{2\pi}{3}\right) \\ &\quad + 2\Delta R_s i_d i_q + \omega_e\left(\Delta L_d i_d^2 - \Delta L_q i_q^2\right) + \omega_e \Delta \psi_f i_d \\ &= \underbrace{2\Delta R_s i_d i_q + \frac{2}{3}R_{\text{add\_}b} i_d i_q + \omega_e\left(\Delta L_d i_d^2 - \Delta L_q i_q^2\right) + \omega_e \Delta \psi_f i_d}_{\text{DC component}} \\ &\quad + \frac{1}{3}R_{\text{add\_}b}\left(i_d^2 + i_q^2\right)\sin\left(2\theta - \frac{\pi}{3}\right). \end{aligned} \tag{33}$$

As seen from (33), as the PMSM operates at a fixed operating point (speed and load), it can be known that the parameter mismatch only influences the dc component in the F_{sum} and has no influence on the second harmonic component in the F_{sum}. In this article, only the second harmonic component in the F_{sum} is used, hence it is deduced that the parameter mismatch has no influence on the performance of the proposed fault diagnosis method. In addition, as the HRC fault occurs in the phases *a* and *b*, the same analysis results can be obtained. Meanwhile, it can be explained, from another aspect, that why the dc component in the F_{sum} is not adopted for the fault diagnosis in this article.

V. Simulation Verification

To validate the proposed method, the simulation is carried out in the MATLAB/Simulink environment. The parameters set for the studied PMSM are listed in Table II. The inverter used in the simulation is the same as that used in the experiment, and the voltage distortions due to the dead-time effect in the *abc* frame are summarized, as shown in Table III. In the simulation, HRC is simulated by adding an additional resistance R_{add} connected in series with one stator winding.

TABLE II
Main Parameters of Studied Surface-Mounted PMSM

Rated Power (W)	750	L_d=L_q (H)	0.035
Rated Current (A)	4.4	PM Flux Linkage (Wb)	0.063
Rated Torque (N.m)	2.39	Rated Speed (r/min)	2000
Number of Pole Pairs	4	Stator Resistance(Ω)	0.7

TABLE III
Specifications for Dead-Time Effect

DC-link (V)	350	Dead-time (us)	3
Switching Frequency (kHZ)	20	Saturation Voltage (V)	2
Switching Device	IGBT (FF300R12ME4)	Forward Voltage (V)	1.65
Turn-on Time (us)	0.17	Turn-off Time (us)	0.45

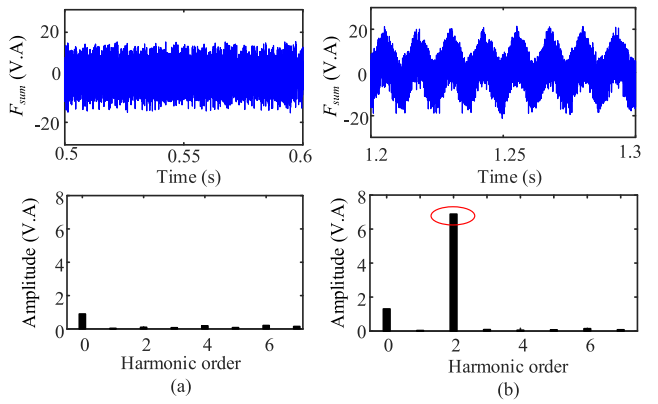

Fig. 4. F_{sum} and FFT results of F_{sum} under healthy and HRC fault conditions. (a) Healthy. (b) HRC in phase *b* ($R_{\text{add\_}b} = 0.5\ \Omega$).

A. Fault Diagnosis and Location

Fig. 4 shows the simulation results under healthy and HRC fault condition, where the PMSM operates at the reference speed 600 r/min with the load of 2 N·m. In addition, in the case of HRC, the fault occurs in phase *b* ($R_{\text{add\_}b} = 0.5\ \Omega$). It can be seen that, as the HRC occurs, the second harmonic component is generated in in the F_{sum}, compared with healthy condition. Additionally, the amplitude of the fundamental component is also increased. It can be seen that the simulation results are in good agreement with the theoretical analysis.

Fig. 5 shows the time-domain waveforms of the stator currents and F_{sum} together with the fault diagnosis information, where the PMSM operates at the reference speed 600 r/min with the load of 2 N·m. At $t = 1$ s, the additional resistance $R_{\text{add\_}b} = 0.5\ \Omega$ is connected in series with stator winding in the phase *b* of the PMSM. It can be seen from Fig. 4 that the estimated resistance rapidly increases, converging to a value of 0.5. The angle θ_f is close to $-\pi/3$. At $t = 1.5$ s, a simultaneous fault in the phases *a* and *b* ($R_{\text{add\_}a} = 0.3\ \Omega$ and $R_{\text{add\_}b} = 0.5$

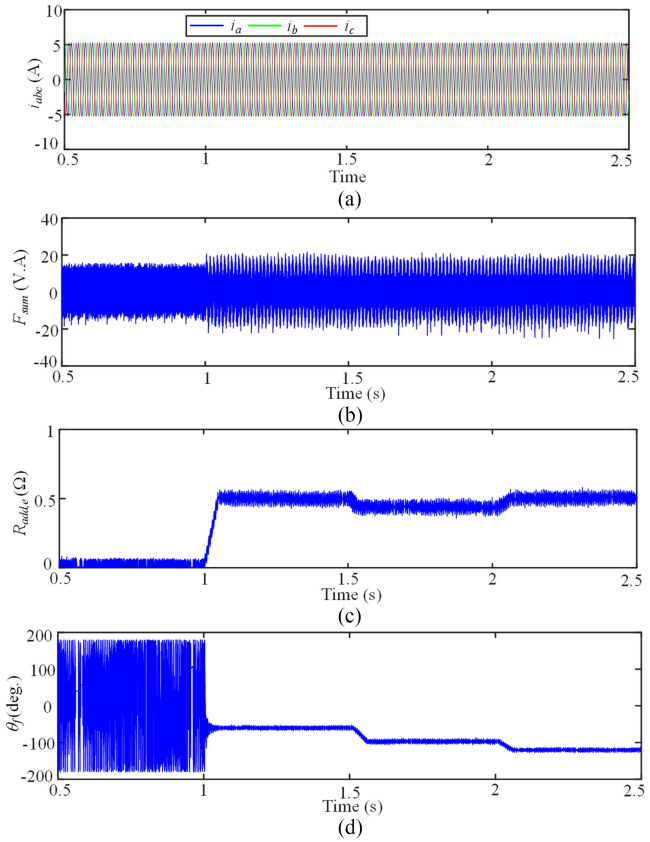

Fig. 5. Simulation results for the HRC in the phases a and b. (a) i_{abc}. (b) $F_{\rm sum}$. (c) $R_{\rm add,}{}_e$. (d) d_c.

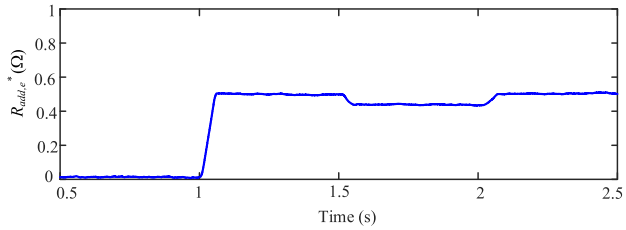

Fig. 6. Mean of sliding window for the HRC in the phases a and b.

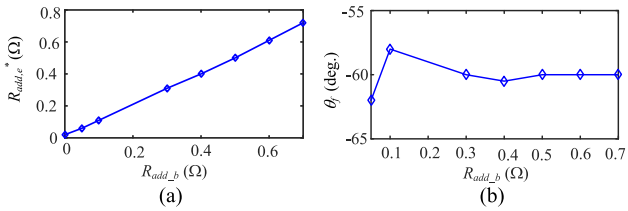

Fig. 7. Fault indicator and initial angle versus additional resistance ($R_{\rm add\_b}$). (a) $R^*_{\rm add,}{}_e$. (b) θ_f.

Ω) is introduced. As a consequence, the estimated resistance converges to a value near to 0.45, and the angle difference θ_f is changed into –5π/9. 0.5 s after the second failure, $R_{\rm add\_a}$ increases to 0.5 Ω and $R_{\rm add\_b}$ is still equal to 0.5 Ω. As a result, the estimated resistance increases to a value near to 0.5, and θ_f is changed into –2π/3. As seen from Fig. 5, the estimated resistance is effectively calculated as the fault occurs in one phase or two phases, and the faults are properly detected through the difference of the estimated resistance between the nonfault and fault states. The value of the angle θ_f is agreed with the theoretical analysis under different conditions and clearly show the faulty phases. Hence, the simulation results show that the proposed method is effective in detecting and identifying the HRC no matter the fault occurring in one phase or two phases.

It is noticed from Fig. 5(c) that the period oscillations appear in the estimated resistance as the fault occurs, which is due to the appearance of the negative sequence current, thus leading to the harmonic with twice stator current frequency in the dq-axis currents i_d and i_q. Hence, a sliding window is adopted to reduce the oscillations, improving the fault diagnosis performance. The mean of the sliding window is defined in (26) and used as a new fault indicator

$$R^*_{{\rm add},e}(k\cdot T_s)=\frac{1}{N}\sum_{i=k-N+1}^{k}R_{{\rm add},e}(i\cdot T_s)\quad N=\frac{T_e}{2T_s} \tag{34}$$

where T_s is the sampling period, T_e is the electrical period of the stator current, and k is an integer.

Fig. 6 shows the mean of sliding window in the case presented in Fig. 5(c). It is shown that the oscillations are obviously decreased, compared with the results in Fig. 5(c).

B. Evaluation of Fault Diagnosis Method

It is important to state that the additional resistance is often set close to the value of the rated phase resistance in the previous studies [23], [35]. In this article, to show the sensitivity of the proposed method, seven different values of the additional resistance are set, namely 7.1% (0.05 Ω), 21.4% (0.15 Ω), 42.8% (0.3 Ω), 57.1% (0.4 Ω), 71.4% (0.5 Ω), 85.7% (0.6 Ω), and 100% (0.7 Ω) of the rated resistance value.

Fig. 7 presents the fault indicator and initial angle versus the additional resistance, where the PMSM operates at the reference speed 600 r/min with the load of 2 N·m. It can be seen from Fig. 7(a) that the fault indicator increases with the increase of the additional resistance, and it is nearly equal to the value of the additional resistance, being in good agreement with the theoretical analysis. Moreover, it is noted that the fault indicator has a high sensitivity to the variation of the additional resistance even for its smaller value (for example, $R_{\rm add\_b}=$ 0.05 Ω), where the fault indicator (equal to 0.06) is larger than the threshold (equal to 0.03), as shown in Fig. 7(a). This indicates that the fault can still be detected even as the value of the additional resistance is smaller. It can be seen from Fig. 7(b) that the initial angle θ_f is hardly affected with the increase in the value of the additional resistance and is always close to –π/3. Hence, the faulty phases can be effectively identified by the initial angle θ_f.

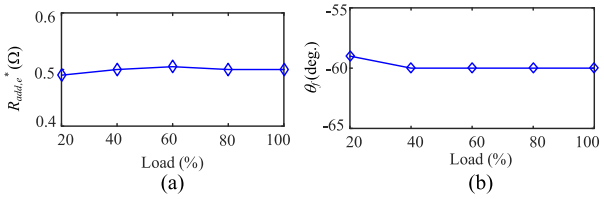

Fig. 8. Fault indicator and initial angle versus load. (a) $R^*_{\mathrm{add},e}$. (b) θ_f.

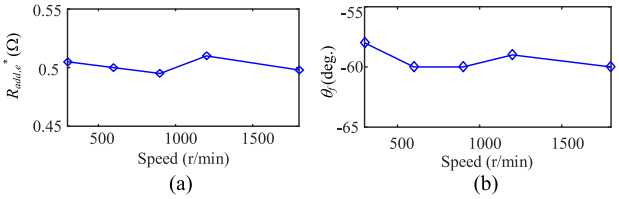

Fig. 9. Fault indicator and initial angle versus speed. (a) $R^*_{\mathrm{add},e}$. (b) θ_f.

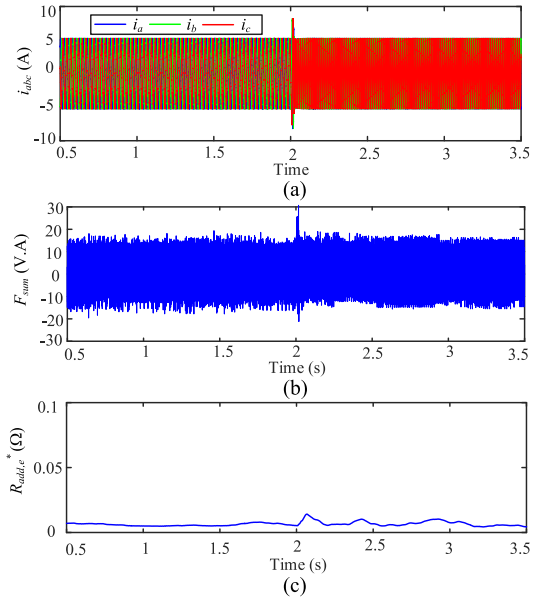

Fig. 10. Simulation results for speed transient.

C. Operating Point

To further validate the proposed fault diagnosis method, the simulation is carried out under different operating points, where $R_{\mathrm{add\_}b} = 0.5\ \Omega$ is connected in series with the phase b.

Figs. 8 and 9 show the simulation results at different loads with the reference speed 600 r/min and at different speeds with the load of 2 N·m, respectively. It can be seen that the operating point has a little influence on the obtained fault indicator and initial angle. Hence, the simulation results show that the proposed method has the good robustness on the operating point.

D. Transient Condition

To verify the performance of the proposed fault diagnosis method, the simulations are performed under transient conditions. Fig. 10 shows the simulation results for the speed transient, where the PMSM is healthy and operates at the load of 2 N·m, and the reference speed is changed from 300 to 1200 r/min at the instant $t = 2$ s. It can be seen that, during the speed transient processes, the stator currents and F_{sum} have the sudden variations, while the fault indicator $R_{\mathrm{add\_}e}$ are hardly influenced by the sudden change of the speed. Fig. 11 shows the simulation results for the load transient, where the PMSM operates at reference speed 600 r/min, and the load is changed from 0.5 to 2 N·m at the moment $t = 2$ s. As seen from Fig. 11, the amplitudes of the stator currents and F_{sum} are increased as the load is changed. However, the fault indicator $R_{\mathrm{add\_}e}$ is hardly influenced by the sudden change of the load.

Hence, the experimental results in Figs. 10 and 11 show that the proposed fault diagnosis method is insensitive to the speed and load transient, and the set threshold (equal to 0.03) allow the proposed fault diagnosis method to deal with the extreme situations (the speed and load transients), being without the false detection.

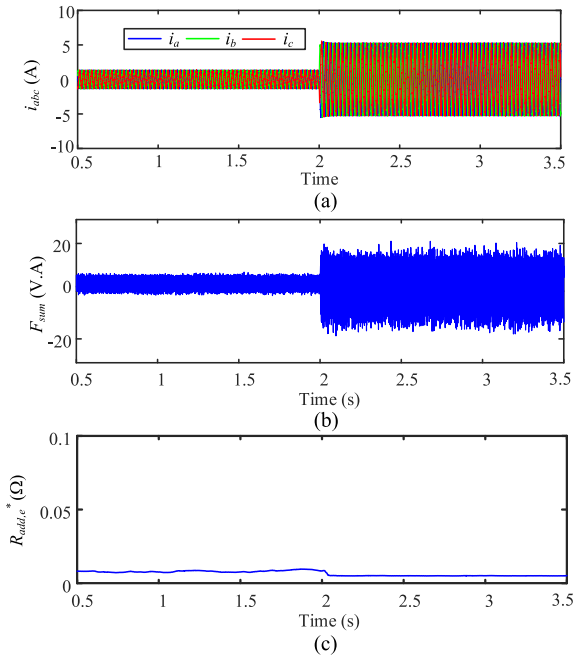

Fig. 11. Simulation results for load transient.

E. Effect of Parameter Mismatch

To further investigate the effect of the parameter mismatch on the proposed fault diagnosis method, the simulations are performed under different situations.

Supposing the dq-axis inductance varies by $\pm 50\%$, i.e., $L_d = 0.5L_d*/L_q = 0.5L_q^*$, $L_d = 1.5L_d*/L_q = 1.5L_q*$, respectively, where L_d^* and L_q^* are the nominal values. The phase resistance also varies by $\pm 50\%$, i.e., $R_s = 0.5R_s*$ and $R_s = 1.5R_s*$. The PM flux linkage also varies by $\pm 50\%$, i.e., $\psi_f = 0.5\psi_f*$ and $\psi_f = 1.5\psi_f*$. Fig. 12 shows the simulation

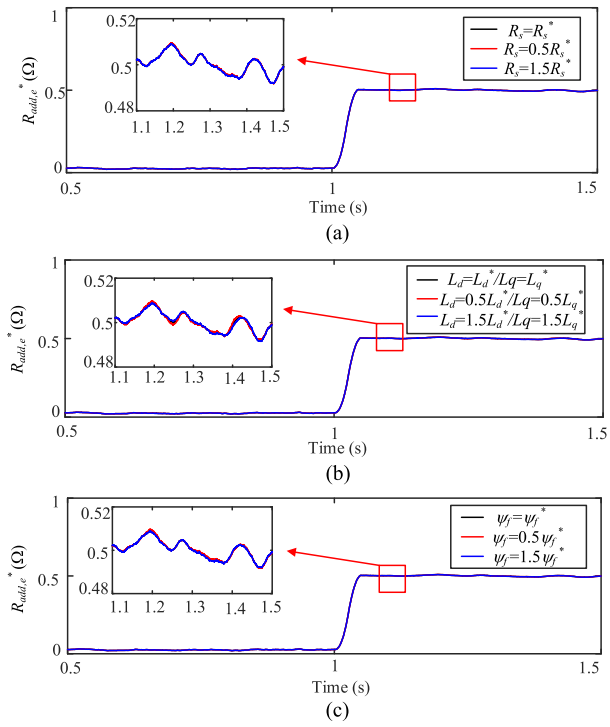

Fig. 12. Simulation results under fault different situations. (a) Variation of phase resistance. (b) Variation of *dq*-axis inductance. (c) Variation of PM flux linkage.

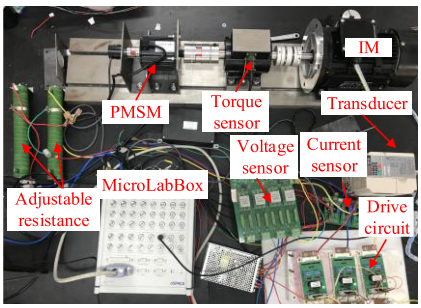

Fig. 13. Experimental platform.

results with different parameters, where the PMSM operates at the reference speed 600 r/min with 2 N·m. Before $t = 1$ s, the PMSM is healthy, and after $t = 1$ s, the HRC fault occurs in the PMSM, where the HRC occurs in phase b ($R_{\mathrm{add\_}b} = 0.5\ \Omega$). As seen from Fig. 9, compared with the case with the nominal values, the fault indicator is hardly varied, showing that the parameter mismatches have little influence on the effectiveness of the proposed fault diagnosis method, which is in good agreement with the theoretical analysis.

VI. Experimental Verification

To further verify the proposed fault diagnosis method, the experimental platform is established, as shown in Fig. 13, mainly including a PMSM, an induction machine (IM), one torque sensor, hardware circuits, a transducer, and MicroLabBox. The PMSM, IM, and torque sensor are coupled together through the couplings, and the IM driven by the transducer is used as the load of the PMSM. The speed information is obtained by an encoder of 1000 pulses per revolution mounted on the rotor shaft end of the PMSM. Together with the MATLAB/Simulink and dSPACE ControlDesk, the MicroLabBox controller provides real-time control and monitoring of the PMSM drive system. The related parameters of PMSM used for the experimental verification are the same as those listed in Table II. In the experiment, the HRC is simulated by adding an additional resistance connected in series with one stator winding.

A. Fault Diagnosis and Location

Fig. 14 shows the experimental results under different conditions, where the PMSM operates at the reference speed 600 r/min with the load of 2 N·m. Fig. 14(a) shows the experimental results under healthy condition. It can be seen that the fault indicator $R_{\mathrm{add},e}*$ is close to 0, and the initial phase angle θ_f is fluctuated in the range from $-\pi$ to π. The experimental results of the HRC in phase b ($R_{\mathrm{add\_}b} = 0.5\ \Omega$) is presented in Fig. 14(b). It is seen that the fault indicator increases, compared with the healthy condition, and it is close to a value of 0.5, and the initial phase angle θ_f is changed and is close to $-\pi/3$. A simultaneous fault occurs in phases a and b, as shown in Fig. 14(c), where $R_{\mathrm{add\_}a} = 0.3\ \Omega$ and $R_{\mathrm{add\_}b} = 0.5\ \Omega$. In this case, the fault indicator is close to the value of 0.44, and the initial angle θ_f is close to $-19\pi/36$. Fig. 14(d) shows the experimental results of the HRC in phase a and phase b ($R_{\mathrm{add\_}a} = 0.5\ \Omega$ and $R_{\mathrm{add\_}b} = 0.5\ \Omega$). As can be seen, the fault indicator is approximately close to the value of 0.5, and the initial phase angle θ_f is close to $-2\pi/3$. From the experimental results, it can be known that both the fault indicator and phase angle have the similar behaviors with the theoretical analysis and the simulation results under different conditions. As the fault occurs in one phase or two phases, both the fault indicator and the phase angle can be accurately estimated. Hence, the HRC fault can be effectively diagnosed through the difference of the fault indicator between the nonfault and the fault states, and the faulty phases can be accurately located by the initial phase angle θ_f. Therefore, the experimental results clearly indicate that the proposed method can effectively achieve the HRC diagnosis and location no matter the fault occurs in one phase or two phases.

B. Evaluation of Fault Diagnosis Method

Fig. 15 presents the fault indicator and initial angle versus additional resistance, where the PMSM operates at the reference speed 600 r/min with the load of 2 N·m. It can be seen from Fig. 15(a) that the fault indicator increases with the increasing of the additional resistance, and it is nearly equal to the value of the additional resistance. Hence, the experimental results indicate that the fault indicator can be also used to assess the fault severity. As seen from Fig. 15(b), the initial angle is hardly influenced by the variation of the additional resistance, showing that the phase angle can be effectively used to locate the faulty phase.

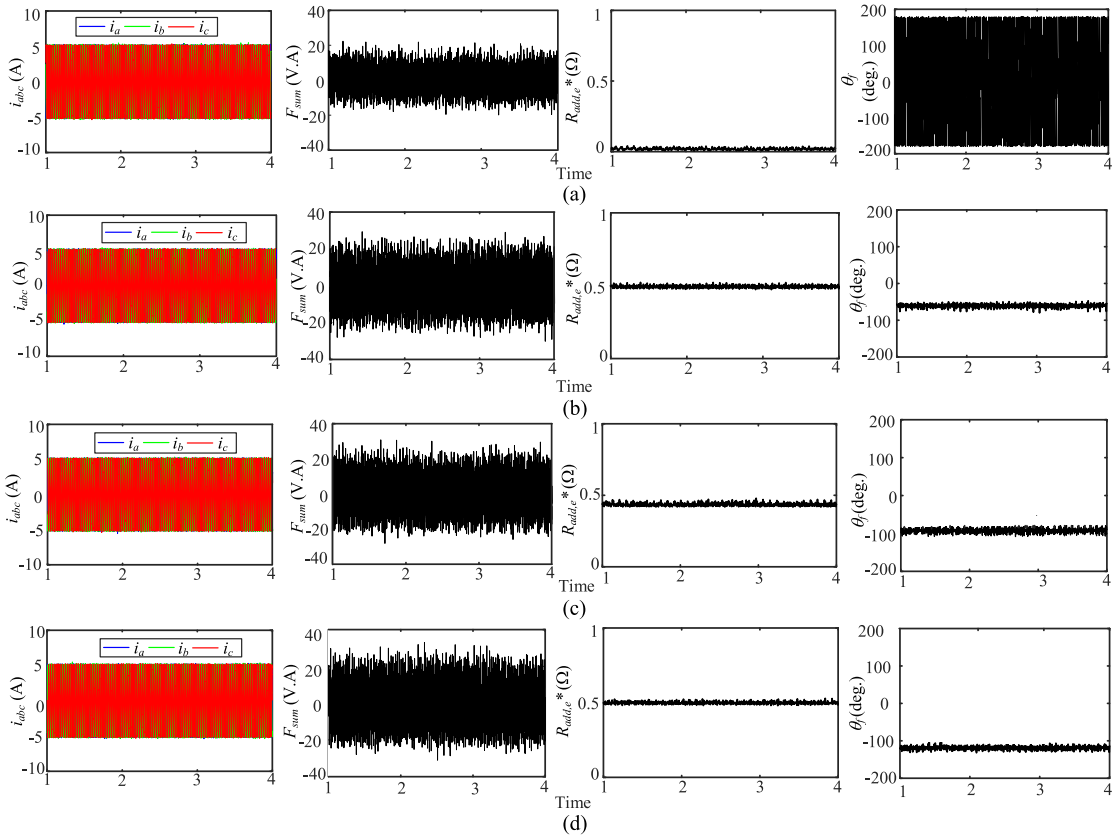

Fig. 14. Experimental results under different conditions. (a) Healthy condition. (b) HRC in phase b ($R_{\mathrm{add\_}b} = 0.5\ \Omega$). (c) HRC in phase a and phase b ($R_{\mathrm{add\_}a} = 0.3\ \Omega$ and $R_{\mathrm{add\_}b} = 0.5\ \Omega$). (d) HRC in phase a and phase b ($R_{\mathrm{add\_}a} = 0.5\ \Omega$ and $R_{\mathrm{add\_}b} = 0.5\ \Omega$).

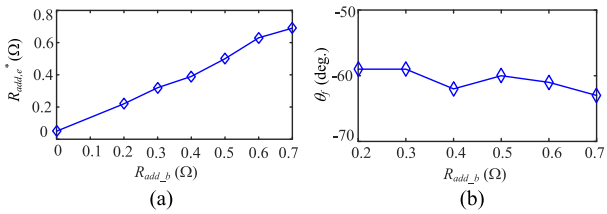

Fig. 15. Fault indicator ($R^{*\mathrm{add},e}$) and angle differences versus additional resistance ($R_{\mathrm{add\_}a}$). (a) $R*_{\mathrm{add},e}$. (b) Angle differences.

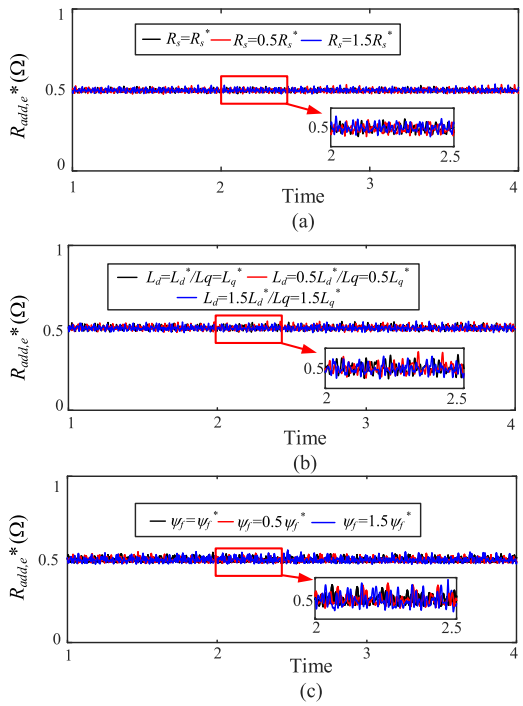

Fig. 16. Experimental results under fault different situations. (a) Variation of phase resistance. (b) Variation of dq-axis inductance. (c) Variation of PM flux linkage.

C. *Effect of Parameter Mismatch*

To further investigate the effect of the parameter mismatch on the proposed fault diagnosis method, the experiments are carried out under different situations. It should be noted that the actual values of the parameters of the experimental prototype can be not easily changed. Hence, in the experiment, the parameter mismatch of the PMSM is simulated by changing the parameters of the voltage distortion estimation method, as expressed in (13) and (14). In addition, the parameter variations of the PMSM are the same as those in the simulation. The dq-axis inductance, the phase resistance, and the PM flux linkage all vary by $\pm 50\%$.

Fig. 16 shows the experimental results with the different parameters, where the PMSM operates at the reference speed 600 r/min with 2 N·m, and the HRC occurs in phase b

($R_{\mathrm{add\_}b} = 0.5\ \Omega$). As seen from Fig. 9, compared with the case with the nominal values, the fault indicator is hardly varied, indicating that the effectiveness of the proposed fault diagnosis method is hardly affected by the parameter mismatches of the PMSM, being in good agreement with the theoretical analysis and simulation results.

Additionally, it can be seen that there is a little difference between the simulation results and experimental ones. It may be caused by the combination of several factors, such as the measurement interference of current sensors, the nonlinearity of the PMSM, and so on. Even so, the simulation and experimental results show that the proposed fault diagnosis method can effectively achieve the fault diagnosis and location of the faulty phases.

VII. Conclusion

This article proposes a model-based strategy with robust parameter mismatch for online HRC diagnosis and localization for PMSM drive system. Both the simulation and experiment results verify the effectiveness of the proposed method. From the theoretical analysis, the simulation and experimental results, the following works and conclusion are drawn.

1) A new fault characteristic signal is defined and is analyzed under different fault condition.
2) Based on the defined signal, the new fault indicators are defined to diagnose the fault and locate the faulty phases.
3) By the fault indicators, the proposed fault diagnosis method not only can detect the HRC, but also can estimate the fault severity and identify the faulty phases, being without requirement of the additional equipment or measurement device.
4) The proposed fault diagnosis method can work under steady state and transient state.
5) The proposed fault diagnosis method is robust against the changes of the PMSM operating point and the parameter mismatch of the PMSM drive system.

References

[1] M. Hermance, Y. Gao, and J. M. Miller, "Hybrid electric vehicles: Architecture and motor drives," *Proc. IEEE*, vol. 95, no. 4, pp. 719–728, Apr. 2007.

[2] M. Cheng and Y. Zhu, "The state of the art of wind energy conversion systems and technologies: A review," *Energy Convers. Manage.*, vol. 88, pp. 332–347, Dec. 2014.

[3] W. Wang, M. Cheng, B. Zhang, Y. Zhu, and S. Ding, "A fault-tolerant permanent magnet traction module for subway application," *IEEE Trans. Power Electron.*, vol. 29, no. 4, pp. 1646–1658, Apr. 2014.

[4] S. Choi *et al.*, "Fault diagnosis techniques for permanent magnet AC machine and drives—A review of current state of the art," *IEEE Trans. Transp. Electrific.*, vol. 4, no. 2, pp. 444–463, Jun. 2018.

[5] J. Yun, J. Cho, S. B. Lee, and J. Y. Yoo, "On-line detection of high-resistance connections in the incoming electrical circuit for induction motors," *IEEE Trans. Ind. Appl.*, vol. 45, no. 2, pp. 694–702, Mar./Apr. 2009.

[6] J. Hang, M. Xia, S. Ding, Y. Li, L. Sun, and Q. Wang, "Research on vector control strategy of surface-mounted permanent magnet synchronous machine drive system with high-resistance connection," *IEEE Trans. Power Electron.*, vol. 35, no. 2, pp. 2023–2033, Feb. 2020.

[7] T. Boileau, N. Leboeuf, B. Nahid-Mobarakeh, and F. Meibody-Tabar, "Synchronous demodulation of control voltages for stator interturn fault detection in PMSM," *IEEE Trans. Power Electron.*, vol. 28, no. 12, pp. 5647–5654, Dec. 2013.

[8] J. Hang, J. Zhang, M. Cheng, and J. Huang, "Online interturn fault diagnosis of permanent magnet synchronous machine using zero-sequence components," *IEEE Trans. Power Electron.*, vol. 30, no. 12, pp. 6371–6740, Dec. 2015.

[9] A. M. Manuel, R. B. Guillermo, H. D. A. Cristian, and R. E. Diego, "A model-based strategy for interturn short-circuit fault diagnosis in PMSM," *IEEE Trans. Ind. Electron.*, vol. 64, no. 9, pp. 7218–7228, Sep. 2017.

[10] H. Jeong, S. Moon, and S. W. Kim, "An early stage interturn fault diagnosis of PMSMs by using negative-sequence components," *IEEE Trans. Ind. Electron.*, vol. 64, no. 7, pp. 5701–5708, Jul. 2017.

[11] W. le Roux, R. G. Harley, and T. G. Habetler, "Detecting rotor faults in low power permanent magnet synchronous machines," *IEEE Trans. Power Electron.*, vol. 22, no. 1, pp. 322–328, Jan. 2007.

[12] B. M. Ebrahimi, M. Javan Roshtkhari, J. Faiz, and S. V. Khatami, "Advanced eccentricity fault recognition in permanent magnet synchronous motors using Stator current signature analysis," *IEEE Trans. Ind. Electron.*, vol. 61, no. 4, pp. 2041–2052, Apr. 2014.

[13] J. Hong, S. B. Lee, C. Kral, and A. Haumer, "Detection of airgap eccentricity for permanent magnet synchronous motors based on the d-axis inductance," *IEEE Trans. Power Electron.*, vol. 27, no. 5, pp. 2605–2612, May 2012.

[14] B. M. Ebrahimi, J. Faiz, and M. J. Roshtkhari, "Static-, dynamic-, and mixed-eccentricity fault diagnoses in permanent-magnet synchronous motors," *IEEE Trans. Ind. Electron.*, vol. 56, no. 11, pp. 4727–4739, Nov. 2009.

[15] K. Kang, J. Song, C. Kang, S. Sung, and G. Jang, "Real-time detection of the dynamic eccentricity in permanent magnet synchronous motors by monitoring speed and back EMF induced in an additional winding," *IEEE Trans. Ind. Electron.*, vol. 64, no. 9, pp. 77191–7200, Sep. 2017.

[16] J. C. Urresty, J. R. Riba, and L. Romeral, "Influence of the stator windings configuration in the currents and zero-sequence voltage harmonics in permanent magnet synchronous motors with demagnetization faults," *IEEE Trans. Magn.*, vol. 49, no. 8, pp. 4885–4893, Aug. 2013.

[17] X. Xiao, C. M. Chen, and M. Zhang, "Dynamic permanent magnet flux estimation of permanent magnet synchronous machines," *IEEE Trans. Appl. Supercond.*, vol. 20, no. 3, pp. 1085–1088, Jun. 2010.

[18] M. Zafarani, T. Goktas, B. Akin, and S. E. Fedigan, "Modeling and dynamic behavior analysis of magnet defect signatures in permanent magnet synchronous motors," *IEEE Trans. Ind. Appl.*, vol. 52, no. 5, pp. 3753–3762, Sep./Oct. 2016.

[19] J. Faiz and E. M. Tehrani, "Demagnetization modeling and fault diagnosing techniques in permanent magnet machines under stationary and nonstationary conditions: An overview," *IEEE Trans. Ind. Appl.*, vol. 53, no. 3, pp. 2772–2785, May/Jun. 2017.

[20] N. M. A. Freier, J. O. Estima, and A. J. M. Cardoso, "A voltage-based approach without extra hardware for open-circuit fault diagnosis in closed loop PWM AC regenerative drives," *IEEE Trans. Ind. Electron.*, vol. 61, no. 9, pp. 4960–4970, Sep. 2014.

[21] J. Hang, J. Zhang, M. Cheng, and S. Ding, "Detection and discrimination of open-phase fault in permanent magnet synchronous motor drive system," *IEEE Trans. Power Electron.*, vol. 31, no. 7, pp. 4697–4709, Jul. 2016.

[22] S. S. Kuruppu and A. Kulatunga, "D-Q current signature based faulted phase localization for SM-PMAC machine drive," *IEEE Trans. Ind. Electron.*, vol. 2, no. 1, pp. 113–121, Jan. 2015.

[23] J. C. Urresty, J. R. Riba, L. Romeral, and J. A. Ortega, "Mixed resistive unbalance and winding inter-turn faults model of permanent magnet synchronous motors," *Elect. Eng.*, vol. 97, no. 1, pp. 75–85, Mar. 2015.

[24] J. Hang, S. Ding, J. Zhang, and M. Cheng, "Fault diagnosis of high-resistance connection in nine-phase flux-switching permanent magnet machine considering neutral-point connection model," *IEEE Trans. Power Electron.*, vol. 32, no. 8, pp. 6444–6454, Aug. 2017.

[25] J. Zhang, J. Hang, S. Ding, and M. Cheng, "Online diagnosis and localization of high-resistance connection in PMSM with improved fault indicator," *IEEE Trans. Power Electron.*, vol. 32, no. 5, pp. 3585–3594, May 2017.

[26] J. Hang, J. Zhang, M. Cheng, and B. Zhang, "High-resistance connection detection in permanent magnet synchronous machine using zero-sequence current component," *IEEE Trans. Power Electron.*, vol. 31, no. 7, pp. 4710–4719, Jul. 2016.

[27] Y. Gritli, A. Tani, C. Rossi, and D. Casadei, "Closed-loop control impact on condition monitoring of high-resistance connections in PMSM based on power signature analysis," in *Proc. 42nd Annu. Conf. IEEE Ind. Electron. Soc.*, Oct. 2016, pp. 6966–6970.

[28] J. Hang, Y. Li, S. Ding, C. Tang, and Q. Wang, "High-resistance connection fault severity detection in a permanent magnet synchronous machine drive system," in *Proc. IEEE 20th Int. Conf. Elect. Mach. Syst.*, 2017, pp. 1–4.

[29] J. Hang, D. Yan, M, Xia, S. Ding, and Q. Wang, "Quantitative fault severity estimation for high-resistance connection in PMSM drive system," *IEEE Access*, vol. 7, pp. 26855–26866, 2019.
[30] J. Hang, H. Wu, S. Ding, W. Hua, and Q. Wang, "A DC-flux-injection method for fault diagnosis of high-resistance connection in direct-torque-controlled PMSM drive system," *IEEE Trans. Power Electron.*, vol. 35, no. 3, pp. 3029–3042, Mar. 2020.
[31] R. Hu, J. Wang, A. R Mills, E. Chong, and Z. Sun, "Detection and classification of turn fault and high resistance connection fault in permanent magnet machines based on zero sequence voltage," *IEEE Trans. Power Electron.*, vol. 35, no. 2, pp. 1922–1933, Feb. 2020.
[32] R. Hu, J. Wang, A. Mills, E. Chong, and Z. Sun, "Detection and classification of turn fault and high-resistance connection fault in inverter fed permanent magnet machines based on high-frequency signals," *J. Eng.*, vol. 17, pp. 4278–4282, Jun. 2019.
[33] S. M. Jung, J. S. Park, H. W. Kim, K. Y. Cho, and M. J. Youn, "An MRAS-based diagnosis of open-circuit fault in PWM voltage-source inverters for PM synchronous motor drive systems," *IEEE Trans. Power Electron.*, vol. 28, no. 5, pp. 2514–2526, May 2013.
[34] H. W. Kim, H. S. Kim, M. J. Youn, and K. Y. Cho, "Online observation and compensation of voltage distortion in PWM VSI for PMSM," *IEE Proc. Elect. Power Appl.*, vol. 151, no. 5, pp. 53–542, Sep. 2004.
[35] Gritli, L. Zarri, C. Rossi, and F. Filippetti, "Advanced diagnosis of electrical faults in wound-rotor induction machines," *IEEE Trans. Ind. Electron.*, vol. 60, no. 9, pp. 4012–4024, Sep. 2013.

Jun Hang (Member, IEEE) received the B.Sc. and M.Sc. degrees from the Anhui University of Science & Technology, Huainan, China, in 2008 and 2011, respectively, and the Ph.D. degree from Southeast University, Nanjing, China, in 2016, all in electrical engineering.

From April 2015 to July 2015, He was a Joint Ph.D. Student with the Department of Energy Technology, Aalborg University, Denmark. Since 2016, he has been with Anhui University, Hefei, China, where he is currently an Associate Professor with the School of Electrical Engineering and Automation. His current research interests include condition monitoring, fault diagnosis, permanent magnet machine and renewable energy. In the recent years, he has authored and coauthored more than 30 technical papers.

Dr. Hang was the recipient of the 1st Prize of 2016 Student Thesis Contest (Ph.D. Category), IEEE Industry Applications Society.

Jibo Zhang received the B.Sc. degree in electrical engineering and automation in 2018 from Anhui University, Hefei, China, where he is currently working toward the M.Sc. degree in electrical engineering.

His current research interests include electrical machine control.

Shichuan Ding (Member, IEEE) received the B.Sc. degree in automation from Anhui University, Hefei, China, in 2001, and the M.Sc. degree from the University of Science and Technology of China, Hefei, China, in 2006, and the Ph.D. degree in electrical engineering from Southeast University, Nanjing, China, in 2018.

Since 2001, he has been with Anhui University, where he is currently an Associate Professor. From 2015 to 2016, he has been a Research Scholar with WEMPEC in University of Wisconsin Madison. In recent years, he has authored and coauthored more than 30 technical papers. His research interests include electrical machine drive, power electronics applications and energy management in EVs and power systems.

Yourui Huang received the B.Eng. degree from the Anhui University of Science and Technology, Huainan, China, in 1994, and the Ph.D. degree from the Anhui Institute of Optics and Fine Mechanics, Chinese Academy of Sciences, Hefei, China, in 2001.

He is currently a Professor in Control Science and Engineering with Anhui University of Science and Technology, Huainan, China. His research interests include intelligent information process and motion control.

Qunjing Wang (Member, IEEE) was born in Bengbu, Anhui, China, in1960. He received the Ph.D. degree in electrical engineering from the Department of Precision Machinery and Precision Instrumentation, University of Science Technology, Hefei, China, in 1998.

From 1983 to 2007, he was with the Hefei University of Technology, Hefei, China. Since 2007, he has been a Professor and a Vice-President at Anhui University, Hefei, China. He also serves as a Research Chair Professor at the National Engineering Laboratory of Energy-saving Motor and Control Technique, Anhui University, China, Power Quality Engineering Research Center of China Ministry of Education, Anhui University, Provincial Collaborative Innovation Center of Industrial Energy-saving and Power Quality Control, Anhui University, China, and Energy-saving Research Institute, Hefei University of Technology. His research interests include motor and drive, converter technology, power quality, and micro grid.

Dr. Wang is the General Chairman of the 11th IEEE Conference on Industrial Electronics and Applications.